FULL PAPER

Functional Selenium Nanoparticles Enhanced Stem Cell Osteoblastic Differentiation through BMP Signaling Pathways

Chuping Zheng, Jinsheng Wang, Yanan Liu, Qianqian Yu, Ying Liu, Ning Deng, and Jie Liu**

Stem cells have generated a great deal of excitement in tissue engineering and regenerative medicine, and it is important to understand the interaction mechanisms between nanomaterials and mesenchymal stem cells (MSCs) for biomedical applications. In this study, ruthenium (II) functional selenium nanoparticles (Ru@Se) are used for stem cell research. Specifically, Ru@Se are compared with citric acid selenium nanoparticles (Cit@Se) to identify their effects on MSCs differentiation and associated molecular mechanism. These data suggest that the effective adsorbing abilities of Ru@Se and Cit@Se allow them to act as preconcentration materials for osteogenic chemical inducers, which accelerates MSCs differentiation into osteoblasts. Further results suggest that selenium nanoparticles enhance the differentiation of MSCs toward osteogenic lineage over adipocytes by promoting osteogenic transcription and attenuating adipogenic transcription. Ru@Se and Cit@Se exert these effects by activating Smad-dependent BMP signaling pathway, which regulates the expression of relevant genes to induce osteogenic differentiation.

1. Introduction

Mesenchymal stem cells are thought to be multipotent cells, which have the ability to proliferate extensively, that can replicate as undifferentiated cells and that maintain the potential to differentiate into multiple cell types in vitro, including bone, cartilage, fat, tendon, muscle, and bone marrow stroma.[1–3] The cultivation and selective differentiation of mesenchymal stem cells (MSCs) could provide further understanding of this important progenitor of multiple tissue types and the potential of new therapeutic ways for the restoration of damaged or diseased tissue. Cells that have the characteristics of human mesenchymal stem cells were isolated from adult bone marrow aspirates. However, for clinical use, MSCs may be detrimental due to the traumatic isolation, high production costs, and the poor supply of bone marrow. The possibility that a decline in the numbers and differentiation potential or plasticity of stem cell populations contributes by aging and age-related disease is suggested to restrict the widespread use of stem cell therapy.[1] With advantages of abundant sources, attainable by a less invasive method, and low production costs, human umbilical cord (HUCMSCs) was introduced as an alternative source for MSCs.[4] Work from several laboratories shows that human umbilical cord mesenchymal stem cells (HUCMSCs) have therapeutic potential, possibly as a substitute cell for bone marrow-derived mesenchymal stem cells for cellular therapy.[5,6]

MSCs can proliferate and be induced to differentiate into osteoblasts, adipocytes, and chondrocytes in vitro. The transdifferentiation of MSCs between osteoblasts and adipocytes is reciprocal, and existing a great extent of plasticity.[7] Increasing evidence suggests a therapeutic opportunity to prevent and treat osteopenic disorders by inhibiting mMSCs adipogenesis and enhancing osteogenesis.[8] MSCs can be induced to differentiate into desired cell types applicable in regenerative medicine and tissue engineering by modifiying substrate topography,[9] material biocompatibility,[10] or applied growth factor inducers. Graphene and graphene oxide have been fabricated to be effective preconcentration platforms for accelerated stem cell growth and differentiation.[11] Although gold nanoparticles and $[Gd@C_{82}(OH)_{22}]_n$ nanoparticles have been showed to be antitumor agents.[12–15] Interestingly, studies demonstrated that they can also enhance the osteogenic differentiation of MSCs.[16,17] This provokes us to study if selenium nanoparticles which are well-known anti-cancer agents have the similar properties.

Selenium, one of the essential trace mineral, is of fundamental importance to human health. Selenium-deficiency

C. Zheng, Dr. Y. Liu, Q. Yu, Y. Liu, Prof. J. Liu
Department of Chemistry
Jinan University
Guangzhou 510632, China
E-mail: tliuliu@jnu.edu.cn
J. Wang, Prof. N. Deng
Guangdong Province Key Laboratory
of Molecular Immunology and Antibody Engineering Biomedicine
Translational
Jinan University
Guangzhou 510632, China
E-mail: tdengn@jnu.edu.cn
Dr. Y. Liu
Department of Applied Biology and Chemical Technology
The Hong Kong Polytechnic University
Hong Kong

DOI: 10.1002/adfm.201401263

diseases have been identified in some areas, where the soil is extremely low in selenium, examples being Keshan disease, an endemic cardiomyopathy, and Kashin-Beck disease, a deforming arthritis.[18] On the other hand, too high levels of selenium in blood could induce toxic effects.[19] It seems closely related to the nature of selenium that too high or too low in selenium would make human or animals suffer pain. Epidemiological studies since the 1970s have provided evidence that low selenium status was associated with a significantly increased risk of cancer incidence and mortality.[20] However, due to the low bioavailability of inorganic selenium, organic selenium in particular nano-selenium is highly valued. In vitro research has shown inhibitory effects of selenium on growth of many cancer cell lines, but not normal cells.[21,22] For instance, our group have synthesized and demonstrated that functional selenium nanoparticles can suppress tumorgenesis and block blood-vessel growth.[23,24] If one were to conclude from earlier work using functionalized nano-conjugates that selenium nanoparticles were toxic at high doses, then important opportunities would have been missed, for example the use of nanorough selenium for promoting healthy osteoblast (bone-forming cell) adhesion.[25] Although the molecular mechanisms governing osteoblast adhesion and self-renewal in the presence of nanoparticles remain unknown, this provokes us to study if they affect bone metabolism by modulating osteogenic differentiation of MSCs.

Herein, we developed a simple fabrication method in which nano-selenium synthesis was carried out in the presence of ruthenium (II) complex $[Ru(bpy)_2(dhipH_3)]^{2+}$ or Citric Acid to functionalize the surface of selenium nanoparticles instead of free selenium nanoparticles in solution, and investigated the effects of functional selenium nanoparticles (Ru@Se, Cit@Se) on the differentiation of HUCMSCs. Cellular assay results demonstrated that Ru@Se and Cit@Se promoted the differentiation of MSCs toward osteoblasts over adipocytes with mineralization of the extra-cellular matrix. Our results suggest that Ru@Se and Cit@Se may serve as preconcentrating materials for the soluble factors necessary for stem cell growth and differentiation, and stimuli on MSCs to activate mechanosensitive signaling pathway in the cells and thus induce osteogenic differentiation. Immunofluorescence, Real-time reverse transcriptase polymerase chain reaction (RT-PCR) and Western blotting assays were designed to verify the hypothesis at the molecular level by determining the expression of genes and proteins related to pathways and the expression of osteogenic and adipogenic biomarkers of MSCs upon interaction with selenium nanoparticles. These results showed that the interaction of MSCs with Ru@Se or Cit@Se may lead to the activation of the Smad-dependent BMP pathway signaling pathway and the up-regulation of p-Smad1/5 protein and the down-regulation of PPARγ adipogenesis specific protein. Interestingly, the results showed that the effect of Ru@Se is stronger than Cit@Se.

2. Results and Discussion

2.1. Preparation and Characterization of Ru@Se and Cit@Se

The synthesis of Ru@Se and citrate functionalized selenium nanoparticles (Cit@Se) are shown in Scheme 1 (Supporting Information). In our method, a luminescent reagent was linked to the surface of nanoparticles by covalent bonding. Specifically, Ru@Se were prepared by reducing $NaSeO_3$ with $NaBH_4$ in the presence of $[Ru(bpy)_2(dhipH_3)]^{2+}$ and citric acid. In this way, phenolic hydroxyl could be employed as a linkage between Ru(II) complex and selenium nanoparticles through forming an O–Se bond. Additionally, the hydroxyl group in Ru(II) complex can serve as a good stabilizer and weak reducing agent.

The morphology and surface state of Ru@Se were characterized by transmission electron microscope (TEM) (**Figure 1**A and Supporting Information Figure S1A). The spherical Ru@Se presented monodisperse and homogeneous spherical structure with an average diameter of about 170 ± 2 nm. The zeta potential of selenium nanoparticles dissolved in physiological saline was about –29.5 mV (Figure S1B, Supporting Information). Using UV–vis spectroscopy, the excitation into the metal-to-ligand charge transfer (MLCT) absorption bands of Ru(II) complex and Ru@Se gave rise to. On the front occasions, MLCT centered emission with λ_{max} at 285 nm and with an acromion at 460 nm (Figure 1C). For Ru@Se, only the absorption peak at 285 nm was observed. The result demonstrated that these were significantly less emissive after adsorption to the Ru@Se surface, for $[Ru(bpy)_2(dhipH_3)]^{2+}$ in the presence of Ru@Se coated with polyphenol monolayers. Ru(II)-polypyridyl complexes are known to have a fluorescent effect. Therefore, further investigation of Ru@Se was carried out by fluorescence spectroscopy. Figure 1B shows fluorescent emission with λ_{max} at 593 and 574 nm for Ru(II) complex and Ru@Se, respectively. We speculate that forming a weak bond between the O of hydroxyl and selenium caused a blue shift of λ_{max}. HRTEM- EDS was used to analyze the elemental composition of Ru@Se. As shown on Figure 1E, there is a strong signal from the Se atoms (33.98%) and Ru atoms (5.04%), respectively. The atomic ratio of Ru/Se was close to 1/6.7. The Cu atom signal (11.80%) was due to the copper-mesh matrix suspending the particles before loading on to the machine. TEM and HRTEM- EDS were also used to investigate Cit@Se (Figure 1D,F). We observed that Cit@Se displayed a good monodisperse structure with an average diameter of about 80 ± 4 nm (Figure 1D and S1B). The distribution of C, O and Se atoms are 22.67%, 17.81%, and 45.10%, respectively.

2.2. Effect of Ru(II), Ru@Se and Cit@Se on Cell Viability and Proliferation

Our previous biocompatibility studies of selenium nanoparticles with cancer cells HepG2 than normal cells HUVEC have shown that the bioeffects of selenium nanoparticles on cancer cells and normal cells were both concentration-dependent. And it's indicated that a higher cytotoxicity of selenium nanoparticles on cancer cells than normal cells, as Rustum et.al found that Se can reduce the toxicity induced by the drugs, such as cisplatin, 5FU, and anthracycline.[26] Therefore, the effect of Ru@Se concentration on the metabolic activity of HUCMSCs, a parameter commonly used to reflect cytotoxicity was first assessed before using Ru@Se as promoter for HUCMSCs osteogenic differentiation. Thus, before determining the role of Ru(II), Ru@Se and Cit@Se in HUCMSC osteogenic and

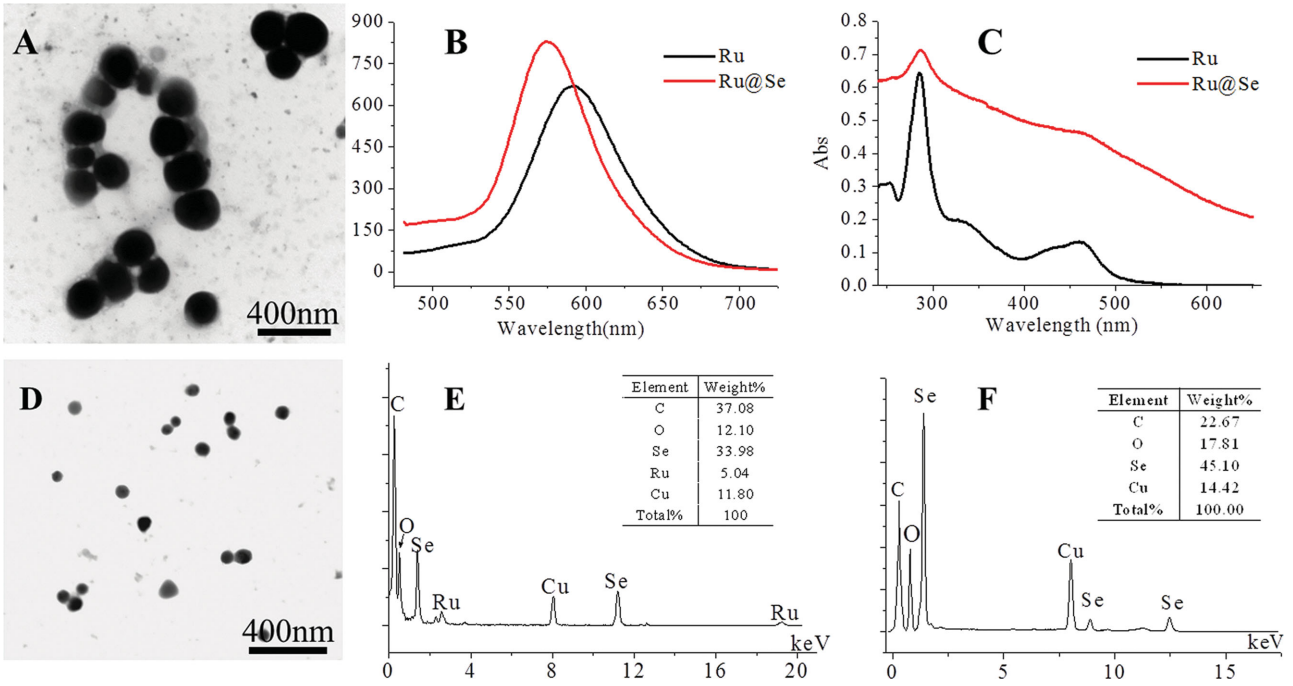

Figure 1. A) TEM image, B) fluorescence spectroscopy, C) UV–vis spectroscopy, and E) EDS image of Ru@Se, respectively. D) TEM image and F) EDS image of Cit@Se.

adipogenic differentiation, we assessed their cytotoxicity via MTT assay. Fluoride is one of the most powerful but least well understood stimulators of bone formation in vivo. Treatment with sodium fluoride has been found that increased proliferation and alkaline phosphatase activity of bone cells in vitro and increased bone formation in embryonic calvaria at concentrations that stimulate bone formation in vivo.[27] Because of the ability to promote osteogenetic differentiation of MSCs, NaF have used as a positive control in maintext. As shown in **Figure 2**B, exposure to Ru(II), Ru@Se and Cit@Se at 2.5, 5, 10, 20, and 40 μg/mL for 72 h caused a slight dose-dependent increase in cytotoxicity compared to the control. Additionally, we found that Ru(II), Ru@Se and Cit@Se showed no change in cytotoxicity at 10 μg/ml with increased exposure time (Figure 2C). These data indicated that the effect of Ru(II), Ru@Se and Cit@Se on HUCMSCs viability and proliferation was dose-dependent. Therefore, Ru@Se were biocompatible with HUCMSCs if the at treatment concentrations less than 10 μg/mL.

In addition, we investigate if Ru(II), Ru@Se, and Cit@Se could induce apoptotic cell death with flow cytometry by using an Annexin-V-FITC / propidium iodide double labeling kit (**Figure 3**A). Incubation of HUCMSCs with Ru(II), Ru@Se, and Cit@Se for 72 h induced 4.6%, 4.2%, and 3.4% apoptosis, respectively. No treatment increased apoptosis or necrosis compared to control cells. These results suggest that Ru(II), Ru@Se and Cit@Se do not induce cell death in HUCMSCs. As cell cycle progression is a critical determinant of cell growth, we also used flow cytometry analysis to investigate whether nanoparticles influenced cell cycle progression in HUCMSCs. As shown in Figure 3B, no cell cycle arrest was observed after treatments with 10 μg/mL Ru(II), Ru@Se, or Cit@Se.

Measurement of ROS generation and oxidative stress can also be used to evaluate drug-induced cytotoxicity.[28] Ru(II) and

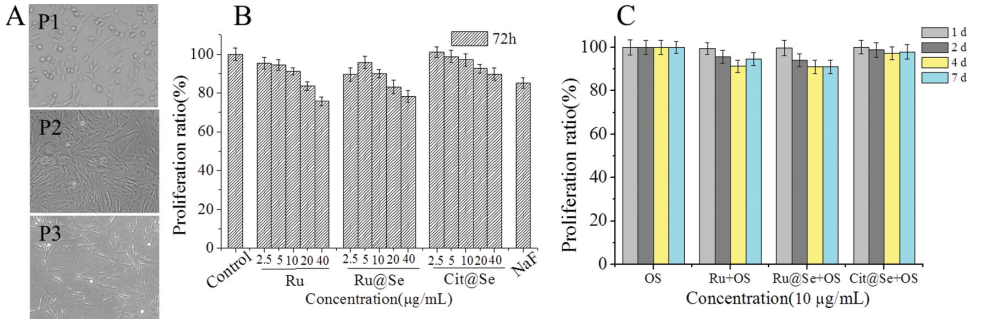

Figure 2. A) Representative optical microscopic images for HUCMSCs at passages 1–3, respectively. B) Cytotoxicity in HUCMSCs exposed to Ru(II), Ru@Se and Cit@Se for 72 h. C) Cytotoxicity in HUCMSCs exposed to Ru(II), Ru@Se and Cit@Se for 1, 2, 4, 7 days, respectively. The cytotoxicity was determined by MTT reduction method.

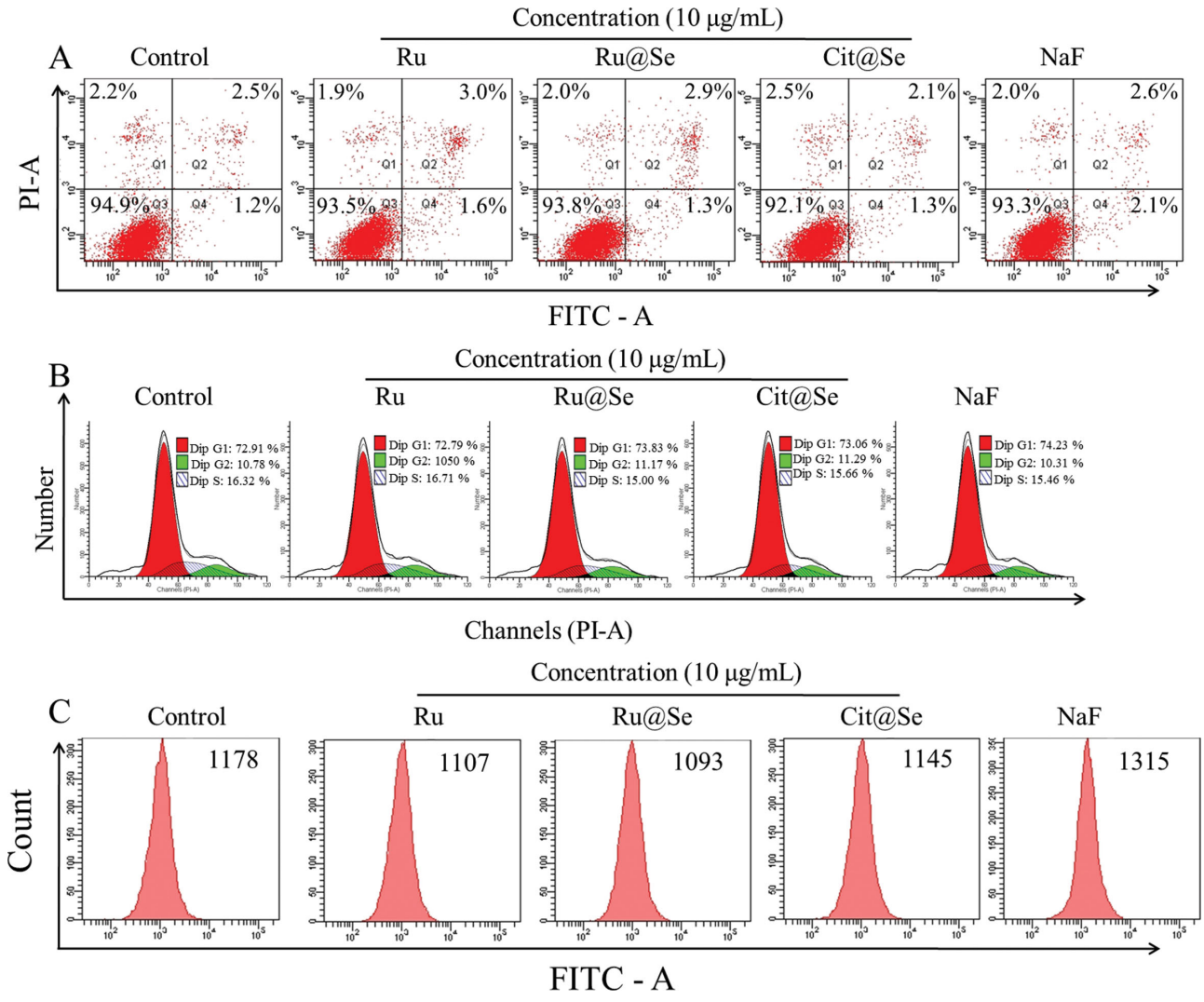

Figure 3. A) Flow cytometry of apoptotic hMSCs as assessed by annexin V-FITC/PI fluorescent intensity. B) Effect on cell cycle distribution of hMSCs. C) Effect on the endogenous ROS level of hMSCs by flow cytometry. In all tests, hMSCs were treated with various materials for 72 h, and 1 mM NaF-treatment was positive control.

selenium nanoparticles have been shown to generate ROS and cause cell apoptosis. Therefore, we measured the intracellular levels of ROS in Ru(II), Ru@Se or Cit@Se -treated HUCMSCs using dichlorofluorescein diacetate (DCFH-DA). In this study, HUCMSCs were serially treated with Ru(II), Ru@Se and Cit@Se at 10 μg/mL for 2 h. As shown in Figure 3C, the results revealed no increased fluorescent signals from DCF compared with the untreated HUCMSCs, suggesting that no ROS were generated by Ru(II), Ru@Se or Cit@Se. After screening the Ru@Se exposure time and concentration creating little cytotoxicity on the HUCMSCs, further experiments were confirmed to investigate if the Ru@Se with 5 μg/mL of concentration had any behavior on the osteogenic differentiation and adipogenic differentiation.

We next used Ru@Se for stem cell labeling. HUCMSCs were incubated with Ru@Se for 12 and 48 h. After washing with PBS to remove free nanoparticles, stem cells labeled with Ru@Se were imaged by a laser scanning confocal microscope. As expected, the HUCMSCs were successfully labeled with Ru@Se and showed quite strong luminescence (Figure S3A). Co-staining for nuclei further validated the localization of Ru@Se signal within the cytoplasm. A time course study of Ru@Se uptake in the cells was carried out by using flow cytometry. HUCMSCs were treated with 10 μg/mL of Ru@Se exposed for 1, 12 and 48 h, respectively. In this assay, untreated HUCMSCs were set as control. As show on the Figure S3B, there are very few cell uptakes when it's exposed for 1 h. And significant cell uptakes can be detected after 48 h exposure time. Figure S3 suggested that the cellular uptake of Ru@Se increased as the rise of time.

2.3. Ru@Se Promoted the Osteogenic Differentiation of HUCMSCs

The osteogenic differentiation of MSCs is a crucial step for osteogenesis.[17] An important sign of MSCs differentiation into osteoblasts is bone matrix mature and mineralization. In this

assay, HUCMSCs were induced to differentiate into osteoblasts in osteogenic supplement (OS) with dexamethasone (10 mM), ascorbate (0.1 mM), and β- glycerolphosphate (10 mM). After 14 days of osteogenic induction, HUCMSCs cultured with Ru(II), Ru@Se and Cit@Se demonstrated greater mineralization than no treatment and NaF treatment controls, as measured by Alizarin Red S staining (**Figure 4**A). Importantly, Ru@Se promoted the greatest mineralization, with Ru@Se, Cit@Se, and Ru(II) promoting mineralization by 28.34%, 21.9%, and 15.68% on day 14, respectively (Figure 4C). Spectrophotometric quantification confirmed these observations by elution of ARS from stained mineral deposits, with significantly higher absorbance at 450 nm (λ_{max}) for HUCMSCs treated with Ru@Se, Cit@Se and Ru(II) as compared to NaF treatment.

It has been reported that there is an inversely proportional relationship between osteogenic and adipogenic differentiation of MSCs.[7] Therefore, we investigated the effects of Ru(II), Ru@Se and Cit@Se on adipocytic differentiation of MSCs. Herein, adipogenic differentiation of HUCMSCs was induced by adipogenic supplement (AS) with dexamethasone (10 μM), indomethacin (0.2 mM), 3-isobuty-1 methylxanthine (IBMX, 0.5 mM) and insulin (4 μg/mL). We determined the adipocytic differentiation rate of HUCMSCs by specifically staining intracytoplasmic lipids with Oil Red O and quantifying expression in situ. Figure 4B, D show adipogenic differentiation of HUCMSCs cultured with Ru(II), Ru@Se and Cit@Se. Our results demonstrated that Ru(II), Ru@Se, and Cit@Se inhibited adipogenic differentiation of HUCMSCs by 27.53%, 31.88%, 35.81%, respectively. In addition, we also investigated the impact of particles to the differentiation capability of HUCMSCs when they culture in basal media. As suggested on Figure S2 (Supporting Information), Ru@Se particles could not induce HUCMSCs osteogenesis and adipogenesis. In short, these data revealed that Ru(II), Ru@Se, and Cit@Se enhanced osteogenic differentiation and inhibited adipogenic differentiation of HUCMSCs, and that the effect of Ru@Se is greater than Ru(II) or Cit@Se.

Given that Ru@Se induced more HUCMSC osteogenic differentiation than Cit@Se, we used ultraviolet spectrophotometry to determine the loading capacities of Ru@Se and Cit@Se for various osteogenic chemical inducers. Previous studies demonstrate that elevated levels of dexamethasone can increase mineral deposition,[29] and dexamethasone is known to alter the expression levels of many proteins and enzymes required during bone differentiation.[30] As presented in Figure S4A-a (Supporting Information), we found that Ru@Se has high adsorption of dexamethasone as compared to Cit@Se. This may be due to the strong drug loading capacity of Se nanoparticles that form a powerful surface adsorption, and the π–π interaction between the aromatic rings of dexamethasone and the polypyridyl ligands of Ru(II) modifier. The chemical structure of citric acid is shown in Scheme 1 (Supporting Information. The molecule contains three carboxylic acid groups that can

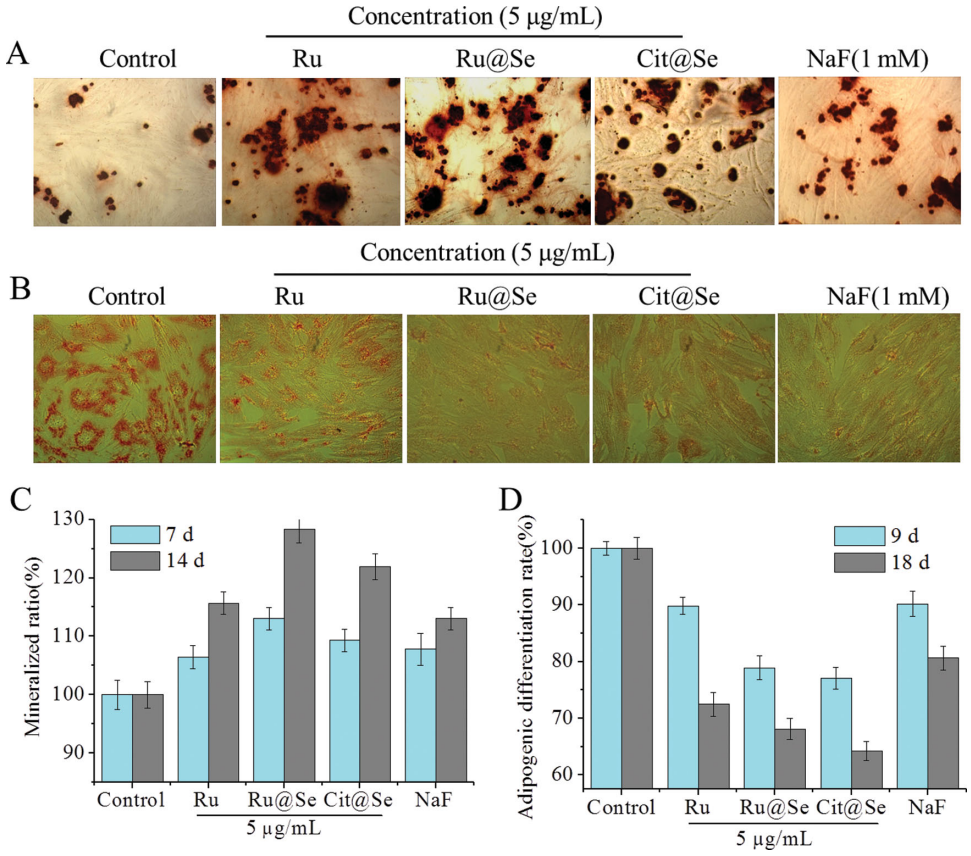

Figure 4. A) Images of Osteogenic differentiation visualized by Alizarin Red staining after 14 days of incubation. B) Extent of cytoplasmic lipid accumulation assessed by Oil Red O staining after 18 days of induction. C) Mineralization quantitated by elution of Alizarin Red S from stained mineral deposits. D) Effects of of different materials on the adipogenic differentiation of MSCs. Results are mean ±SD of the triplicate experiments.

bind to selenium.[31] Moreover, the carboxylic acid groups can also mediate binding to dexamethasone through the hydrogen bonding between the carboxyl groups and fluorine atom of dexamethasone. Although the hydroxyl group on citric acid is much shorter than carboxyl groups, it also makes contribution to binding with dexamethasone. Because of the bingding ability on the surface of Cit@Se, a slight dexamethasone adsorption of Cit@Se was also observed. Taken together, the promoted osteogenic differentiation of HUCMSCs following Ru@Se treatment may be attributed to the increased local concentration of adsorbed dexamethasone.

Notably, dexamethasone is not the sole chemical that is responsible for inducing the osteogenic differentiation of hMSCs. Studies showed that dexamethasone acted synergistically with β-glycerolphosphate and intracellular alkaline phosphatase enzyme to synthesize new mineralized bone matrices.[32] Figure S4A-b (Supporting Information) shows the significant adsorption of β-glycerolphosphate by Ru@Se and Cit@Se. This suggests that high adsorption of β-glycerolphosphate with enough adsorbed dexamethasone is required to enhance hMSCs differentiation into osteogenic lineages. The large surface loading capacities of Ru@Se and Cit@Se may be responsible for the high adsorption of β-glycerolphosphate. Additionally, as depicted in Figure S4A-c (Supporting Information), our results show high adsorption of ascorbic acid on Cit@Se and Ru@Se, This may be due to the degree of hydrogen bonding between the –OH moieties of the ascorbic acid and the citrate. On the other hand, another functional group Ru(II) complex on Ru@Se has slightly obstructed the adsorption effect of Ru@Se. Together, our results suggest that Ru@Se enhanced the osteogenic differentiation of HUCMSCs via effective loading of various osteogenic chemical inducers. Since insulin is the main mediator for fatty acid synthesis, we measured the adsorption isotherms of insulin by Cit@Se and Ru@Se. Figure S4A-d (Supporting Information) shows that Ru@Se exhibited the lower adsorption capacity as compared to Cit@Se.

Insulin is one of the major factors in promotion the adipogenic differentiation of stem cell.[33] Circular dichroism spectroscopy (CD) was used to investigate the potential causes for Ru(II), Ru@Se and Cit@Se inhibition of adipogenesis (**Figure 5**B). CD spectroscopy the attenuated negative absorption peaks of insulin at 210.0 and 225.2 nm corresponding to the α-helix and β-pleated sheets, respectively (Figure S4B-a, Supporting Information). The results suggest significant differences between Ru(II), Ru@Se, and Cit@Se interactions with insulin compared to NaF controls. We speculate that the weak alkaline of NaF (1 mM, pH = 7.1) is close to PBS, which can stabilize insulin. The CD data suggests there is no interaction of NaF with insulin, which can be judged from the attenuated negative absorption peaks at 210.0 and 225.2 nm without change (Figure S4B-a, Supporting Information). However, upon incubation with Ru@Se for one day, the peak corresponding to β-pleated sheets decreased until unobservable at day 3 (Figure S4B-b, Supporting Information). We believe the discrepancy observed in the CD absorption profile is not a result of self-aggregation of insulin by recording its high tension voltage curves.[11] Instead, it can be attributed to the

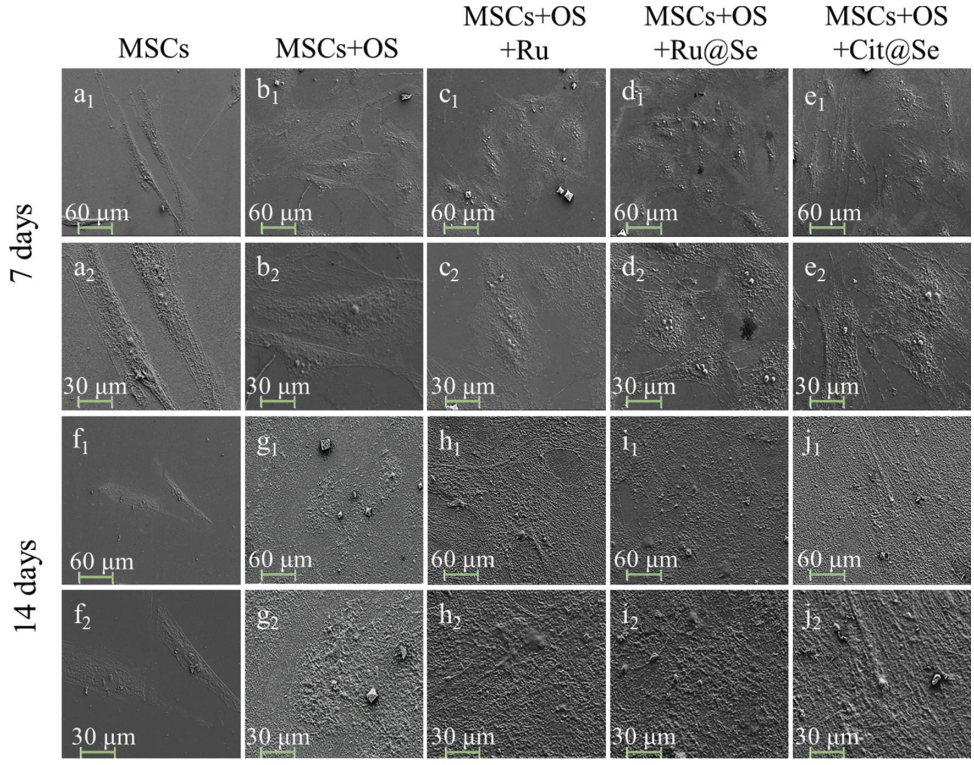

Figure 5. FSEM images of MSCs after 7 and 14 day culture. a1,a2,f1,f2) MSCs were cultured in normal media. b1,b2,g1,g2) MSCs were cultured in OS media. c1,c2,h1,h2) MSCs were cultured in presence of OS and Ru(II). d1,d2,i1,i2) MSCs were treated with OS and Ru@Se. e1,e2,j1,j2) MSCs were treated with OS and Cit@Se.

conformational changes of insulin caused by Ru@Se incubation and subsequent reduced HUCMSC differentiation into adipocytes. As presented in Supporting Information Figure S4B-c,d, Ru(II) and Cit@Se did not change the structure of insulin, but influenced its CD signal intensity. Overall, UV–vis and CD data suggest that the effective loading abilities of Ru@Se allow it to act as a preconcentration material for osteogenic chemical inducers.

2.4. Morphological Analysis by Field Scanning Electron Microscopy (FSEM)

When cultured in basal medium, MSCs flattened and expanded cytoplasmic extensions over the entire surface and the cells displayed a spindly, fibroblast-like morphology and formed clusters, which is the normal phenotype behavior of hMSCs (Figure 5a1,a2,f1,f2). FSEM was used to investigate the morphological changes of HUCMSCs following osteogenic induction for 7 and 14 days. As the cells differentiated into osteoblasts in the presence of OS with and without Ru(II), Ru@Se, or Cit@Se treatment for 7 days, the HUCMSCs surface was covered with a network of well-spread cells with a more polygonal morphology (Figure 5b1-e1). High magnification FSEM images revealed long pseudopodia cells with various sizes and shapes (Figure 5b2-e2), and the effect is more significant in the presence of Ru(II), Ru@Se and Cit@Se, suggesting that these materials promoted osteoblast functionality. HUCMSCs cultured in OS medium with nanoparticle treatment for 14 days showed multilayered polygonal osteocyte-like cells that elaborated a highly dense network of mineralized nodules throughout the construct (Figure 5h1–2, j1–2). Together, our FSEM data strongly demonstrated a substantial promotion of osteogenic differentiation of HUCMSCs upon their interactions with Ru(II), Ru@Se, and Cit@Se.

2.5. Ru@Se Elevated Osteogenic Specific Gene Expression in MSCs

Several studies using an RNA interference approach provided the evidence for the involvement of genes (OCN, BMP, Runx2 etc.) in osteogenic or adipogenic differentiation of MSCs. Semi-quantitative RT-PCR and quantitative real-time PCR (Q-PCR) experiments were carried out to analyze osteospecific and adipospecific gene expression from HUCMSCs cultured in osteogenic and adipogenic media with PBS, NaF, Ru(II), Ru@Se, or Cit@Se treatment for 14 days (**Figure 6**). Beta-actin mRNA was used as reference. The relative amount of mRNA expression were normalized according to ACTB ($2^{-\Delta\Delta Ct} = 1$) using the comparative CT ($2^{-\Delta\Delta Ct}$) methods and the fold-change is in respect to control (OS group). As expected, osteoblast specific genes, including ALP, BMP-2, OCN, OPN, Col I, and Runx2, were up-regulated in HUCMSCs treated with Ru, Ru@Se, or Cit@Se during osteogenic differentiation as compared to the OS group (Figure 6A). In addition, osteoblast specific genes showed highest expression in HUCMSCs treated with Ru@Se, suggesting that the effects of Ru@Se on osteogenic differentiation were greater than with other nanoparticles (Figure 6A,B). In contrast, adipose specific genes CEBPα, CEBPβ, CEBPΔ, and PPARγ were significantly down-regulated as compared to the AS group (Figure 6C). Interestingly, mRNA expression of adipospecific genes in HUCMSCs treated with Ru@Se was down-regulated to an extremely low level. Therefore, compared with Ru(II) and Cit@Se, Ru@Se promoted more osteogenic differentiation and less adipogenic differentiation of HUCMSCs, consistent with the observed effects of Ru@Se on mineralized matrix nodule formation (Figure 4A) and Oil red staining of HUCMSCs (Figure 4B). As indicated in **Figure 7**A,B, gene expression of HUCMSCs cultured with Ru(II) were not significantly different from those on Cit@Se during osteogenic differentiation and adipogenic differentiation.

Based on real-time PCR results, ALP was up-regulated by 5.57 folds (Figure 6B). ALP is a calcium- and phosphate-binding protein and a phosphor-hydrolytic enzyme that plays a major role in bone mineralization and is considered to a phenotypic marker for osteoblast cells. Runx2 showed a 2.47-fold up-regulation when HUCMSCs were treated with Ru@Se (Figure 6B). Runx2 is known to play a vital role in regulating both embryonic bone development and postnatal osteoblastic function. Previous work demonstrates that Runx2 expression stimulates mesenchymal cells to differentiate into osteoblasts and inhibits their differentiation into chondrocytes and adipocytes.[34] Runx2 can also up-regulate the expression of bone matrix genes, including OCN, OPN, fibronectin, Col I and bone sialoprotein (BSP). Col I showed a 3.90-fold increase when HUCMSCs were treated with Ru@Se (Figure 6). Col I is the most abundant protein of the extracellular bone matrix and has an important role in influencing cellular behavior. In bone formation, OPN is an important marker of bone remodeling, but it is not identified as a bone-specific protein since it is expressed in other types of tissues.[35] In contrast, OCN is expressed in differentiating cells of intermediate and mature nodules and is the most specific gene for mineralization and osteoblastic differentiation.

Furthermore, our results also demonstrated that Ru@Se appeared to have a stronger inhibitory effect than Cit@Se on adipogenic differentiation of HUCMSCs. According to the Q-PCR results, Ru@Se inhibited adipogenic differentiation by down regulating the expression of adipose specific genes CEBPα, CEBPβ, CEBPΔ and PPARγ to 0.3, 0.16, 0.23, and 0.4 fold, respectively (Figure 6C,D). It is well known that adipogenesis is a highly regulated process with a cascade of dynamic events involving many factors. In addition, CCAAT/enhancer-binding proteins (CEBPs), a family of six transcription factors including CEBPα and CEBPβ, is critical for adipogenic differentiation in tissues.[36] Peroxisome proliferator-activated receptor-γ (PPARγ), a nuclear receptor, is known as the master regulator of adipocyte biology. Previous research has shown that both CEBPα and CEBPβ are required along with PPARγ for robust adipocyte-specific gene expression. Additonally, the majority of adipocyte genes is not regulated by PPARγ alone but rather requires CEBPα and CEBPβ as well.

In the presence of Ru@Se, up-regulated expression of BMP2 was observed during osteogenic differentiation (Figure 7). Many studies have demonstrated that BMP/Smad signaling plays a critical role in postnatal bone homeostasis including osteoblast expansion, differentiation, and bone formation.[37] Therefore, we speculated that osteogenic differentiation of HUCMSCs might be linked to Smad activity and transcriptional changes of

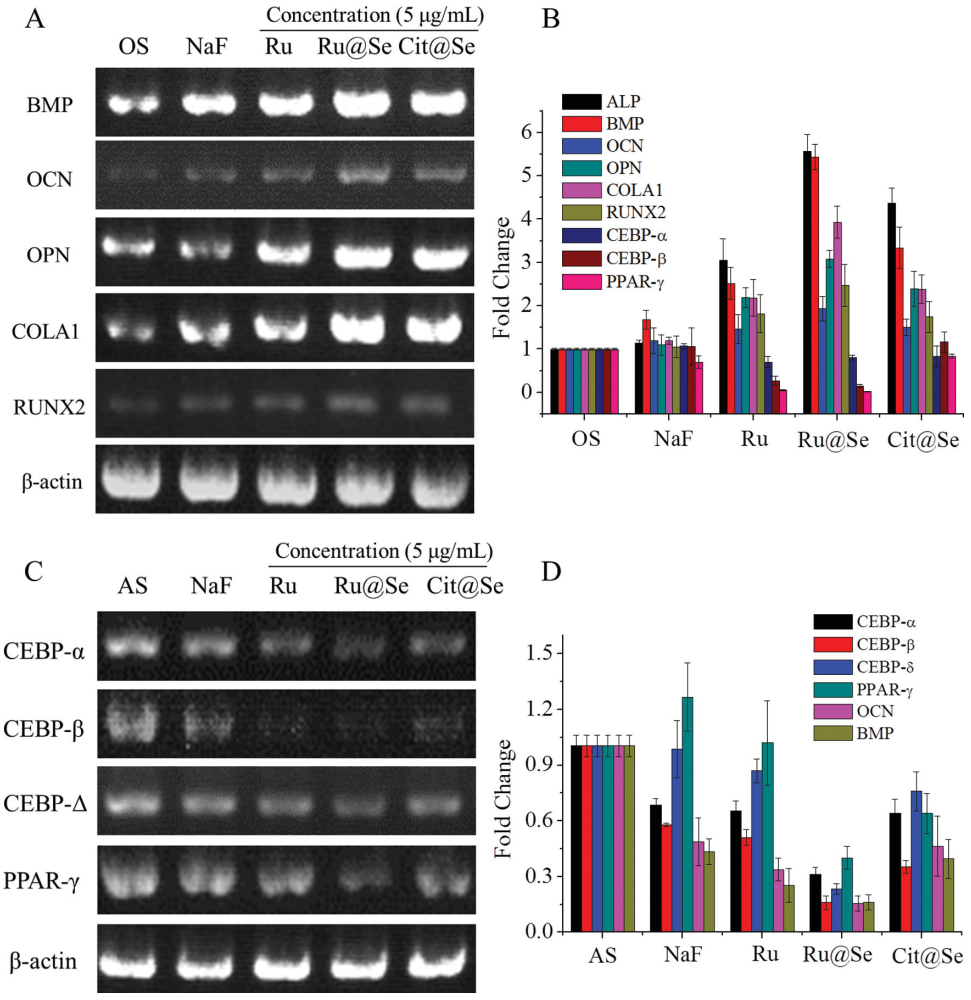

Figure 6. A,C) Semi-quantitative RT-PCR and B,D) quantitative real-time PCR analysis of osteogenic and adipogenic specific gene expression in MSCs upon treatment with 5 μg/mL Ru(II), Ru@Se, and Cit@Se. 1 mM NaF set as positive control. Values are the mean±SD of three independent experiments.

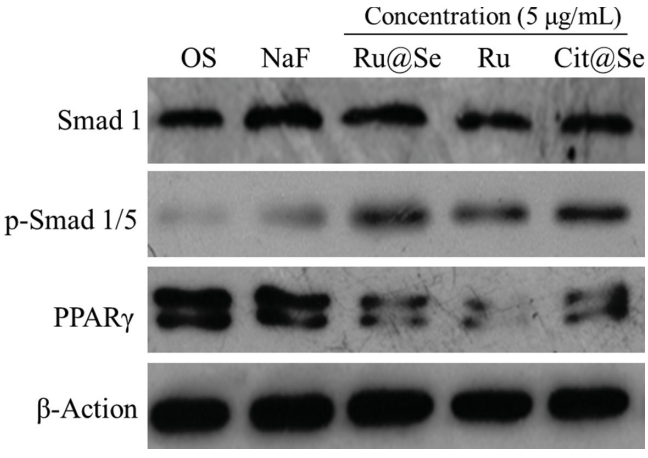

Figure 7. Western blot analysis for Smad1, p-Smad1/5, and PPARγ proteins in HUCMSCs treated with Ru@Se, Ru, and Cit@Se after 7 day incubation, respectively. 1 mM NaF- treatment set as positive control. β-Actin protein expression as a loading control. Proteins from each lysate were separated in SDS-PAGE.

its target genes in the BMP signaling pathway. Consistent with our PCR results, Western blot analysis indicated that Ru@Se significantly increased the expression of phosphorylated Smad proteins (p-Smad1/5) during osteogenic differentiation and inhibited PPARγ protein expression during adipogenic differentiation as compared to other groups (Figure 7). We speculate that Ru@Se upregulation of BMP promoted BMP binding to its receptor on the cell surface, and subsequent receptor kinase activation increased Smad1/5 phosphorylation. Phosphorylated Smad1, 5, or 8, with Smad4, then formed a complex and translocated into the nucleus, where they regulate the transcription of BMP target genes. Together, our Western blot and Q-PCR results confirmed osteogenic differentiation was dramatically enhanced whereas the differentiation of adipocytes was inhibited with Ru@Se treatment.

2.6. Phenotype Analysis

Our Alizarin red staining suggests that Ru@Se promoted osteogenic differentiation and mineralization of the hMSCs in

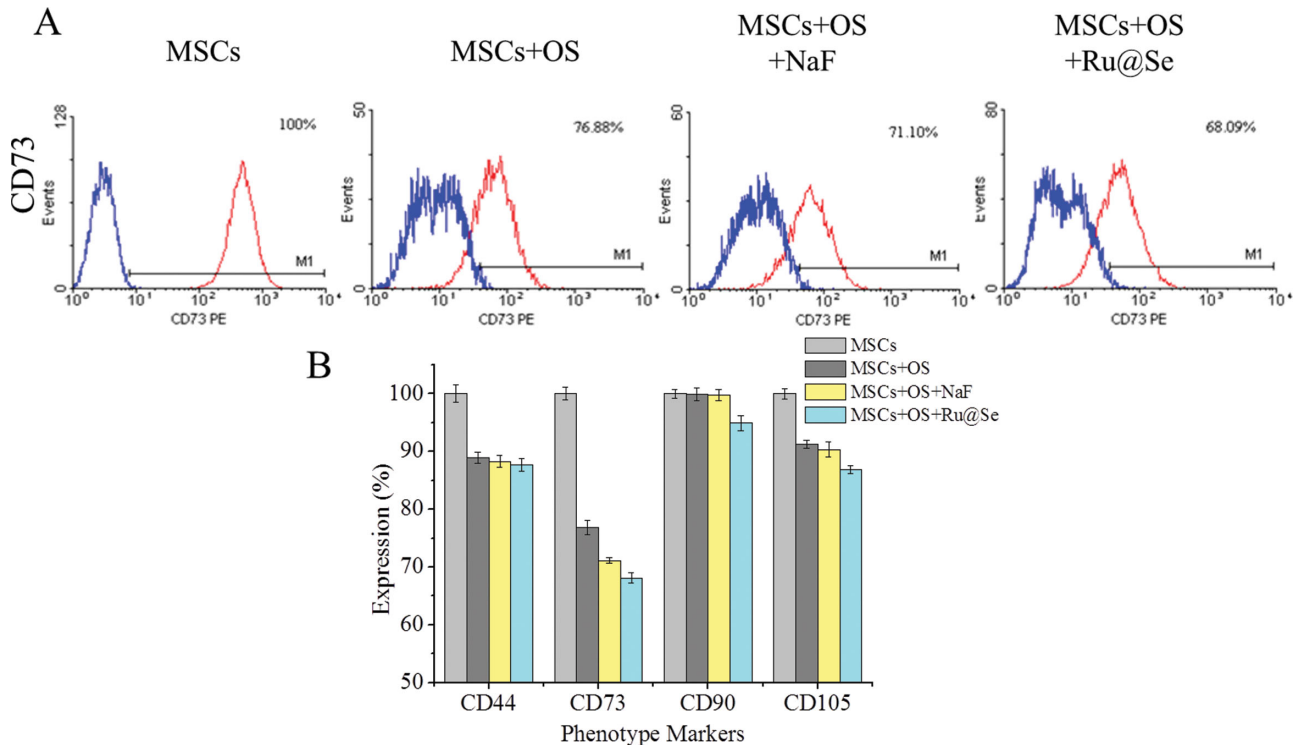

Figure 8. Flow cytometric analysis of hMSCs lineage marker: CD44, CD73, CD90, and CD105. Values are the mean±SD of three independent experiments.

vitro. To further evaluate cell phenotype changes during osteogenic differentiation, MSCs-related markers such as CD44, CD73, CD90, CD105, were measured by flow cytometry when HUCMSCs were induced in osteogenic medium with Ru@Se treatment for 14 days. Many researches have been reported that CD44 expression is one of the characteristics of MSCs in both humans and mice.[38] In addition, the changes in CD44 expression on the cell surface could result in changes in differentiation potential and other cellular processes of the cultured MSCs. Recent research indicated that through CD73 antagonist treatment, the mineral matrix deposition of MSCs was almost completely abolished and osteogenic differentiation marker expression decreased.[39] It is likely that CD90 is expressed during proliferation but expression level declines as MSCs mature towards osteoblast-like cells. Our flow cytometery results indicate that the addition of Ru@Se markedly inhibited the expression of CD73 when compared with OS media without nanoparticles (**Figure 8**A). On the other hand, the percentages of CD44, CD90 and CD105 were markedly reduced to 87.67%, 94.95% and 86.89%, respectively (Figure 8B). These results suggested that the isolated HUCMSCs had already begun differentiation, and Ru@Se sped up the process of differentiation.

2.7. Immunofluorescence Analyses

Substantial research efforts have shown that the Smad1-dependent BMP pathway is one of most important signaling pathways to promote osteogenic differentiation.[40] This conclusion is consistent with our results of Q-PCR and western blot. To further demonstrate the influence of Ru@Se on BMP signaling pathway, we treated HUCMSCs with Noggin, a BMP signaling inhibitor. Western blot analyses revealed that Ru@Se increased Smad1/5 phosphorylation in HUCMSCs and Noggin treatment blocked this increase (**Figure 9**A,B). The apparent reduction of p-Smad1/5 in the cytoplasm and nucleus was confirmed in Ru@Se and Noggin-treated cells by immunofluorescent staining (Figure 9C). Our results suggested that Ru@Se significantly promoted the osteogenic differentiation of HUCMSCs through the BMP pathway, although in some studies there are many signaling pathways other than Smad pathways involved in osteoblast differentiation.[41] As depicted in Figure S5, the expression levels of PPARγ was reduced with Ru@Se treatment of HUCMSCs during adipogenic differentiation.

3. Conclusions

In this study, we used HUCMSCs as a model to determine the efficacy of Ru@Se in stem cell differentiation. Our results indicate that the concentration and incubation time of Ru@Se can be optimized to achieve efficient MSC differentiation into osteoblasts with negligible cytotoxicity. Specifically, 10 μg/mL Ru@Se treatment did not negatively impact the proliferation of MSCs. Flow cytometry experiments showed that Ru@Se did not induced cell cycle arrest or result in cellular ROS generation. In order to determine Ru@Se suitable for stem cell labeling, we next carried out cellular uptake and localization studies of nanoparticles using confocal fluorescence microscopy. After incubation for 12 h and 48 h, we observed luminescence in the stem cells, demonstrating that the HUCMSCs were successfully labeled with Ru@Se. Co-staining for nuclei further validated

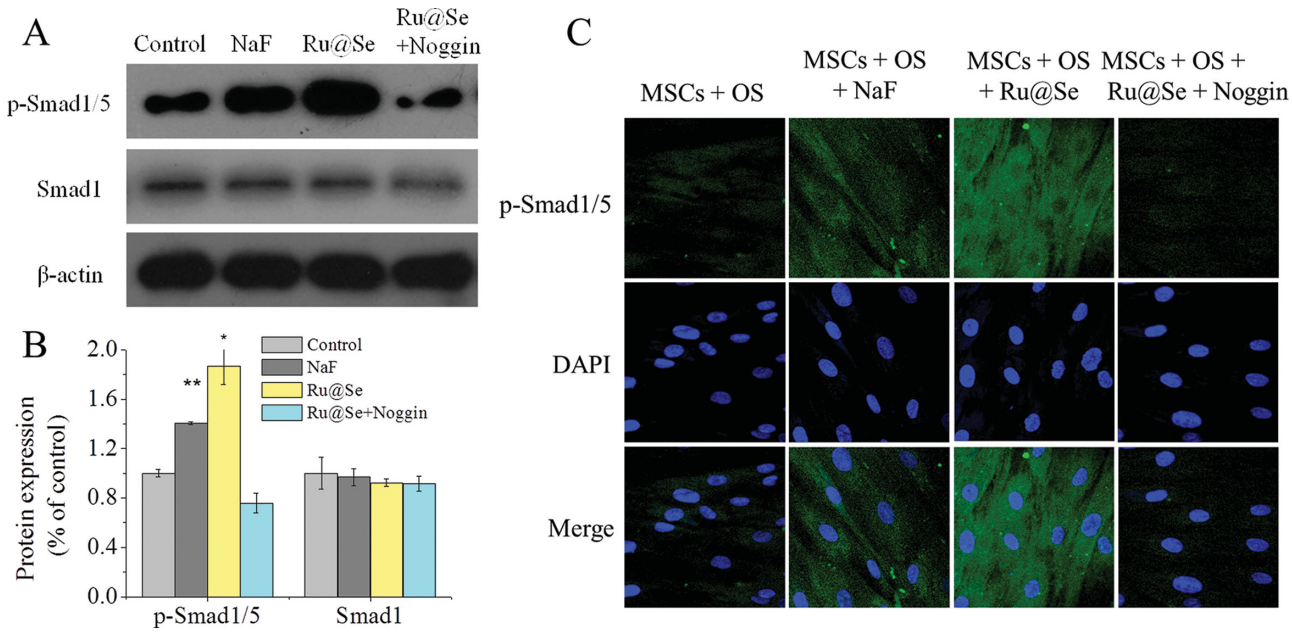

Figure 9. Ru@Se effects on HUCMSCs differentiation. A) Western blot analysis for Smad1 and p-Smad1/5 proteins in hMSCs after 7 day incubation. B) Immunofluorescence images of MSCs treated with Ru@Se (5 μg/mL). Noggin was used as a BMP signaling pathway inhibitor.

the localization of Ru@Se signal within the cytoplasm. This supports the feasibility of Ru@Se for in vivo cell tracking.

Ru@Se treated HUCMSCs exhibited less adipogenic differentiation and more osteogenic differentiation than controls. It is well-known that the BMP signaling pathway plays an important role in osteogenic differentiation of MSCs.[42] **Figure 10** proposes a plausible mechanism for Ru@Se's osteogenic effects on HUCMSCs. The enhancement of MSCs osteogenesis likely excite the BMP signaling pathway by interacting between Ru@Se and proteins, such as BMP receptors, at the cell membrane or in the cytoplasm, such as the promotion of R-Smad phosphorylation. As showed in Figure S3A (Supporting Information), confocal images validated the localization of Ru@Se signal within the cytoplasm. And it is well agreed with the schematic model. Western blotting results revealed the expression levels of key proteins involved in the BMP signaling pathway, such as Smad1 and p-Smad1/5, were significantly increased. This data suggests that Ru@Se activates the BMP pathway during the osteogenic differentiation. Moreover, BMP signaling inhibitor noggin[17] decreased p-Smad1/5 levels enhanced by Ru@Se.

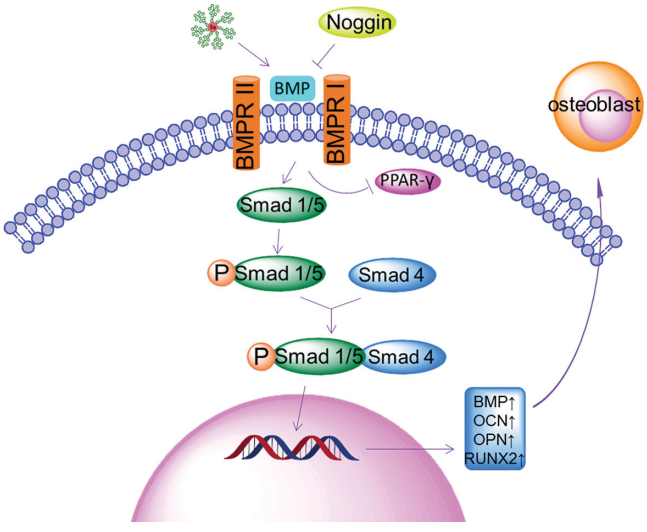

Figure 10. Molecular mechanism of the modulation of osteogenic differentiation of HUCMSCs by Ru@Se through BMP and MAPK signaling pathway

Taken together, the data presented here shows that synthetic Ru@Se are cytocompatible and can enhance osteogenic differentiation of MSCs. Additionally, Ru@Se can be served as a potential labeling agent to track stem cells. In this study, we demonstrate that Ru@Se can work as preconcentrating materials responsible for the soluble factors necessary for stem cell growth and differentiation. Moreover, Ru@Se activates the BMP signaling pathway through upregulating the level of p-Smad1/5 protein, and facilitates osteogenic differentiation efficiency. The ability of Ru@Se to accelerate stem cell differentiation suggested that Ru@Se could be very promising for bone engineering and applications.

4. Experimental Section

Synthesis and Characterization of Ru@Se and Cit@Se: A Na_2SeO_3 stock solution (0.1 M) was prepared by dissolving 1.7294 g of Na_2SeO_3 (Sigmae-Aldrich Chemical) in 100 mL of purified water. $NaBH_4$ and Citric Acid were purchased from Shanghai Reagent, China. Ruthenium (II) complexes (denoted as $[Ru(bpy)_2(dhipH_3)]^{2+}$) was obtained from our previous work. A 0.1 mM stock solution of $[Ru(bpy)_2(dhipH_3)]^{2+}$ was prepared by dissolving $[Ru(bpy)_2(dhipH_3)]^{2+}$ in Milli-Q water and kept at 4 °C. Selenium nanoparticles (denoted as Ru@Se) were prepared via the reduction of Na_2SeO_3 and $NaBH_4$ in the presence of $[Ru(bpy)_2(dhipH_3)]^{2+}$. As-prepared Ru@Se[43,44] was subsequently

characterized by transmission electron microscope (TEM) (JEM-2010, JEOL, Japan), UV/visible spectroscopy, high resolution transmission electron microscopy (HRTEM) and fluorescence spectroscopy. Another selenium nanoparticle was also prepared by the same way in the presence of Citric Acid (denoted as Cit@Se).

Isolation and Culture of MSCs: Human umbilical cords were harvested from Guangzhou Overseas Chinese Hospital after normal deliveries. Pregnant women were informed and gave consent, and the protocol for tissue procurement was approved by the Institutional Review Board of Jinan University. In brief, the umbilical cords vessels were removed, and the mesenchymal tissue was minced into 1–2 mm^3 cubes, then incubated with 0.2% collagenase type II (Sigma, MO, USA) for 2 h at 37 °C, finally passed through a 100 μm filter to collected cell suspensions. The centrifuged cell pellets were re-suspended in Human Umbilical Cord Mesenchymal Stem Cell Growth Medium (Cyagen Biosciences Inc., Catalog No. HUXUC-90011) and then plated in T-75 cell culture flasks. Cultures were maintained at 37 °C, in a humidified incubator with 5% CO_2. After 3 days of culture, the growth medium was replaced and the remnants of the cord fragments were removed. The umbilical cord mesenchymal stem cells (HUCMSCs) were cultured until they reached to 80% confluence. The HUCMSCs isolated at passages 3–5 were used in this research. As presented in Figure 2A, there are the microscope images of HUCMSCs at passages 1–3, respectively.

MTT Assay: In brief, HUCMSCs were seeded in 96-well culture plates at a density of 2×10^4 cells/well and incubated for 72 h. After incubation, Ru (II), Ru@Se, and Cit@Se were added to the wells at concentrations of 2.5, 5, 10, 20, and 40 μg/mL. Cells without selenium nanoparticles or Ru (II) complex treatment were used as control group. And NaF-treatment was used as positive control. The proliferation ratio of control is set as 100%, and the proliferation rate of test group (in percent) was calculated according to the formula: $OD_{sample}/OD_{control} \times 100\%$.

Mineralized Matrix Formation Assay: The HUCMSCs were seeded in a 12-well plate and cultured for 7 and 14 days in DMEM with 10% FBS. Control groups were prepared in the presence of osteogenetic induction supplement (OS) only, and the positive control was prepared by addition of 1 mM NaF. Alizarin Red S (ARS) staining was used to examine the formation of mineralized matrix nodules. In brief, the cells were fixed with 4% paraformaldehyde for 30 min at room temperature. Then washed with PBS 3 times and stained with 40 mmol-1 ARS, pH 4.2 for 30 min at room temperature. The mineralized matrix formation rate (%) was calculated according to the formula: $OD_{sample}/OD_{control} \times 100$.

Oil Red O Staining Assay for Adipogenic Differentiation: The HUCMSCs were seeded in 12-well tissue culture plates and cultured for 9 and 18 days. The adipogenetic induced supplements and drugs were added to the culture medium. Oil Red O staining assay was used to evaluate adipogenic differentiation of HUCMSCs. The adipogenetic differentiation inhibition was expressed as a percentage of $[OD_{sample} - OD_{blank}]/[OD_{control} - OD_{blank}] \times 100$.

Apoptosis Analysis: Apoptosis was detected with an annexin V-FITC kit purchased from TOYOBO (Japan) according to the manufacturer's instructions. 1×10^6 HUCMSCs were seeded in 6-well culture dishes and allowed to grow for 24 h at 37 °C/5% CO_2. The cells were treated with Ru(II), Ru@Se and Cit@Se for 24 h, respectively. Then collected, suspended in 200 μL of binding buffer. Subsequently, 5 μL of FITC-labeled annexin V and 5 μL of the PI stock solution were added to the cell suspension for 15 min in the dark at room temperature. Stained cells were analyzed with a flow cytometry (BD FACSAria).

Measurement of Intracellular ROS: The intracellular ROS level of drugs-treated HUCMSCs was measured using ROS assay kit following the manufacturer's instruction. The HUCMSCs treated with or without Ru(II), Ru@Se, and Cit@Se were washed with PBS. Then, the cells were harvested and incubated in the dark with DCFH-DA (10 mmol/mL) for 20 min at 37 °C. DCFH excitation and emission wavelengths were at 488 and 525 nm, respectively, and the fluorescence intensity was detected using flow cytometry (BD FACSAria). The positive control was prepared by addition of 1 mM NaF.

Cell Cycle Analysis: HUCMSCs were also seeded in 6-well culture dishes and allowed to grow for 72 h of incubation. Then cells were washed, harvested, and fixed with 70% ethanol overnight. After incubation with a PI solution for 30 minutes at 4 °C in the dark, cell cycle distributions were analyzed using flow cytometry (BD FACSAria).

Cell Uptakes: HUCMSCs were cultured in the presence of basal media with Ru@Se- treatment for 12 and 48 h. The cell nucleuses were counterstained with DAPI (Sigma-Aldrich). Then cells were washed with PBS and observed by using confocal microscopy ((LSM700, Carl Zeiss, Germany). In flow cytometry assay, HUCMSCs were treated with 10 μg/mL of Ru@Se exposed for 1, 12, and 48 h, respectively. The time course study of Ru@Se uptake in the cells was carried out by using flow cytometry on a BD FACScan flowcytometry system.

Adsorption of Chemical Inducers by Nanoparticles: 10 mM dexamethasone, 1 M β-glycerophosphate, 0.1 M ascorbic acid, and 10 mM insulin were prepared in phosphate buffer. Ru@Se, Cit@Se nanoparticles and Ru(II) complex (10 mg/mL) in PBS were sonicated for 1 h prior to usage, and form a homogeneous dispersion. The chemical agents were mixed with Ru(II), Ru@Se and Cit@Se (volume ratio 1:1) and stirred up to 4 h at room temperature. NaF- treatment was prepared as a positive control. After which, each mixture was centrifuged at 10 000 rpm for 30 min. The supernatant was collected, and the adsorption isotherm of the respective chemical agent was obtained by UV-vis spectroscopy in wavelength range of 200–350 nm on day 1 and 3. The amount of adsorption for each chemical inducer was determined based on the change in protein adsorption before and after the addition of Ru(II), Ru@Se, and Cit@Se.

Circular Dichroism Spectroscopy: CD spectra experiments were carried out on a JASCO J-810 spectropolarimeter in wavelength range of 200~260 nm. The scanning speed was set at 500 nm/min, and the optical path length was set as 1 nm. All samples were prepared in PBS in advance on day 1,3. Three scans were accumulated and automatically averaged.

Field Scanning Electron Microscope (FSEM): Cell morphology with and without NPs- treatment was observed by FSEM after 7 days of culture. HUCMSCs were collected and washed in PBS three times and subsequently fixed in 2.5% glutaraldehyde for 2 h and dehydrated through a graded series of ethanol. The dehydrated HUCMSCs were vacuum dried in desiccators for overnight. After mounted onto aluminum stubs, and sputter coated with gold. SEM imaging was conducted on scanning electron microscope system (S-4500; Hitachi, Japan) at an accelerating voltage of 20 kV.

Real-Time Quantification PCR analysis (Q-PCR): Total RNA from human umbilical cord mesenchymal stem cells (HUCMSCs) in the presence of OS or AS for 14 days which was extracted using RNAiso Plus (Takara Code:D9108A) and was reverse transcribed to complementary DNA (cDNA) according to the TaKaRa protocol. PCR reaction (20 μL) of cDNA was carried out using Blend Taq plus DNA Polymerase (TAKARA) following the instructions of the manufacturer. Semi-quantitative RT-PCR conditions were as follows: 3 min at 95 °C, followed by 30 cycles of 10 s denaturation at 95 °C, 30 s annealing at 58 °C, and 30 s extension at 72 °C. The gene-specific primer sequences are listed in Table 1 (Supporting Information).These genes included osteoblast specific genes, ALP, BMP2, OCN, OPN, COLA1, and RUNX2, and adipose specific genes, CEBPα, CEBPβ, CEBPΔ, and PPARγ. PCR products were analyzed electrophoretically by 1% agarose gel using the BIO-RAD GelDoc 2000 (BIO-RAD). The mRNA expression were also quantitatively characterized according to real-time quantification PCR (Q-PCR) using SYBR Premix Ex TaqTM (TaKaRa Code:DRR041A) and MiniOpticon Real–Time PCR Detection System (Model CFB-3120, BIO-RAD). The PCR began with 3 min at 95 °C, followed by 40 cycles of 10 s at 95 °C, 30 s at 58 °C and 30 s at 72 °C, and later followed by the melting curve test. The relative amount of mRNA expression were normalized according to ACTB ($2^{-\Delta\Delta Ct} = 1$) using the comparative CT ($2^{-\Delta\Delta Ct}$) methods.

Western Blot Analysis: Cells were lysed in cold RIPA buffer (VETEC, #V900854) containing 1 mM PMSF for 30 min and scraped the cells off the plate immediately. The extract was transferred to a micro-centrifuge tube and centrifuged at 12 000 *g* for 15 min at 4 °C. Equal amounts of protein from each sample subjected to SDS-PAGE using 10% gel and electro-transferred to Immobilon-P membranes (Millipore, Bedford, MA). After transfer, washed Immobilon-P membranes with 25 mL PBST

for 5 min and incubated membrane in 25 mL of 5% bovine serum albumin in PBST solution (137 mM NaCl, 2.7 mM KCl, 10 mM Na_2HPO_4, 2 mM KH_2PO_4, 0.05% Tween-20) for 2 h at room temperature. Following incubation with primary antibodies against Smad1, p-Smad1/5, Erk1/2, p-Erk1/2, PPARγ, β-Actin (all from CST), and HRP-linked goat anti-rabbit IgG (CST,) as the secondary antibody, protein bands were visualized with chemiluminescent HRP Substrate kit (Millipore, Billerica, MA, p90719). Proteins were detected by exposure to Kodak X-ray film (hekang, China) in the proper exposure time, which were subsequently scanned with an HP 200 scanner (Palo Alto, USA).

Flow Cytometry: HUCMSCs were cultured in the presence of osteogenetic supplement (OS) with and without NPs- treatment for 7 days. Then, cells were stained with fluorochrome-conjugated antibodies specific for the following surface markers: CD44, CD73, CD90 and CD105 for 1 h at room temperature in the dark. The samples were washed by centrifugation in 2 mL incubation buffer, re-suspended in 0.5 mL 1× PBS and analyzed by flow cytometry on a BD FACScan flowcytometry system. Data analysis was conducted with WinMDI29 software (The Scripps Research Institute, La Jolla, CA).

Immunofluorescence: HUCMSCs were grown on coverslips at a density of 1×10^5 cells well-1 at 37 °C for 24 h. Then the media was replaced with 2 mL osteogenic or adipogenic media in the presence or absence of nanoparticles. After 2 weeks of induction, the cells were washed 3 times in PBS for 5 minutes each. After being fixed with 4% paraformaldehyde for 0.5 h, subsequently permeabilized with 0.3% Triton X-100 in PBS for 10 min. Then, PPARγ Rabbit mAb (CST, #2443) or Phospho-Smad1/5 Rabbit mAb (CST, #9516) was incubated overnight at 4 °C. Follow by incubation with Anti-Rabbit- Alexa Fluor 488 (CST, #4412) or Anti-Rabbit-Alexa Fluor 555 (CST, #4413) for 1 hours at room temperature in dark, the nucleus were counterstained with DAPI (Sigma-Aldrich). Rinse three times in PBS for 5 minutes each. The specimens were examined by using confocal microscopy ((LSM700, Carl Zeiss, Germany).

Acknowledgements

C.Z. and J.W. contributed equally to this work. This work was supported by the National Natural Science Foundation of China (21171070, 21371075), the Planned Item of Science and Technology of Guangdong Province (c1211220800571), and the Fundamental Research Funds for the Central Universities.

Received: April 19, 2014
Revised: July 9, 2014
Published online: September 1, 2014

[1] M. F. Pittenger, A. M. Mackay, S. C. Beck, R. K. Jaiswal, R. Douglas, J. D. Mosca, M. A. Moorman, D. W. Simonetti, S. Craig, D. R. Marshak, *Science* **1999**, *284*, 143–147.
[2] A. Singh, J. Zhan, Z. Ye, J. H. Elisseeff, *Adv. Funct. Mater.* **2013**, *23*, 575–582.
[3] Y. Jiang, B. N. Jahagirdar, R. L. Reinhardt, R. E. Schwartz, C. D. Keene, X. R. Ortiz-Gonzalez, M. Reyes, T. Lenvik, T. Lund, M. Blackstad, *Nature* **2002**, *418*, 41–49.
[4] S. Kern, H. Eichler, J. Stoeve, H. Klüter, K. Bieback, *Stem Cells* **2006**, *24*, 1294–1301.
[5] K. Bieback, S. Kern, H. Klüter, H. Eichler, *Stem Cells* **2004**, *22*, 625–634.
[6] R. Taghizadeh, K. Cetrulo, C. Cetrulo, *Placenta* **2011**, *32*, S311–S315.
[7] C. Song, Z. Guo, Q. Ma, Z. Chen, Z. Liu, H. Jia, G. Dang, *Biochem. Biophys. Res. Commun.* **2003**, *308*, 458–462.
[8] M. Nuttall, J. Gimble, *Bone* **2000**, *27*, 177–184.
[9] M. J. Dalby, N. Gadegaard, R. Tare, A. Andar, M. O. Riehle, P. Herzyk, C. D. Wilkinson, R. O. Oreffo, *Nat. Mater.* **2007**, *6*, 997–1003.
[10] A. J. Engler, S. Sen, H. L. Sweeney, D. E. Discher, *Cell* **2006**, *126*, 677–689.
[11] W. C. Lee, C. H.Y. Lim, H. Shi, L. A. Tang, Y. Wang, C. T. Lim, K. P. Loh, *ACS Nano* **2011**, *5*, 7334–7341.
[12] D. Du, S. Liu, J. Chen, H. Ju, H. Lian, J. Li, *Biomaterials* **2005**, *26*, 6487–6495.
[13] C. R. Patra, R. Bhattacharya, D. Mukhopadhyay, P. Mukherjee, *Adv. Drug Delivery Rev.* **2010**, *62*, 346–361.
[14] C. Chen, G. Xing, J. Wang, Y. Zhao, B. Li, J. Tang, G. Jia, T. Wang, J. Sun, L. Xing, *Nano Lett.* **2005**, *5*, 2050–2057.
[15] Y. Liu, F. Jiao, Y. Qiu, W. Li, F. Lao, G. Zhou, B. Sun, G. Xing, J. Dong, Y. Zhao, *Biomaterials* **2009**, *30*, 3934–3945.
[16] C. Yi, D. Liu, C.-C. Fong, J. Zhang, M. Yang, *ACS Nano* **2010**, *4*, 6439–6448.
[17] K. Yang, W. Cao, X. Hao, X. Xue, J. Zhao, J. Liu, Y. Zhao, J. Meng, B. Sun, J. Zhang, *Nanoscale* **2013**, *5*, 1205–1212.
[18] C. Reilly, Selenium in food and health, 1st ed., Blackie Academic & Professional, London; New York **1996**.
[19] M. P. Rayman, *Lancet* **2012**, *379*, 1256–1268.
[20] M. P. Rayman, *Lancet* **2000**, *356*, 233–241.
[21] S. Apostolou, J. O. Klein, Y. Mitsuuchi, J. N. Shetler, P. I. Poulikakos, S. C. Jhanwar, W. D. Kruger, J. R. Testa, *Oncogene* **2004**, *23*, 5032–5040.
[22] D. G. Menter, A. L. Sabichi, S. M. Lippman, *Cancer Epidem. Biom. Prev.* **2000**, *9*, 1171–1182.
[23] D. Sun, Y. Liu, Q. Yu, Y. Zhou, R. Zhang, X. Chen, A. Hong, J. Liu, *Biomaterials* **2013**, *34*, 171–180.
[24] D. Sun, Y. Liu, Q. Yu, X. Qin, L. Yang, Y. Zhou, L. Chen, J. Liu, *Biomaterials* **2014**, *35*, 1572–1583.
[25] J. Holinka, M. Pilz, B. Kubista, E. Presterl, R. Windhager, *Bone Joint J.* **2013**, *95*, 678–682.
[26] J. Mishra, J. Drummond, S. H. Quazi, S. S. Karanki, J. Shaw, B. Chen, N. Kumar, *Criti. Rev. Oncol. Hematol.* **2013**, *86*, 232–250.
[27] J. Wergedal, D. Baylink, *Science* **1983**, *222*, 330–332.
[28] A. E. Nel, L. Mädler, D. Velegol, T. Xia, E. M. Hoek, P. Somasundaran, F. Klaessig, V. Castranova, M. Thompson, *Nat. Mater.* **2009**, *8*, 543–557.
[29] N. Jaiswal, S. E. Haynesworth, A. I. Caplan, S. P. Bruder, *J. Cell. Biochem.* **1997**, *64*, 295–312.
[30] H. Oshina, S. Sotome, T. Yoshii, I. Torigoe, Y. Sugata, H. Maehara, E. Marukawa, K. Omura, K. Shinomiya, *Bone* **2007**, *41*, 575–583.
[31] D. S. Kilin, O. V. Prezhdo, Y. Xia, *Chem. Phys. Lett.* **2008**, *458*, 113–116.
[32] O. Akhavan, E. Ghaderi, M. Shahsavar, *Carbon* **2013**, *59*, 200–211.
[33] M. Wabitsch, P. B. Jensen, W. F. Blum, C. T. Christoffersen, P. Englaro, E. Heinze, W. Rascher, W. Teller, H. Tornqvist, H. Hauner, *Diabetes* **1996**, *45*, 1435–1438.
[34] T. Komori, *Front. Bios.: J. Virtual Library* **2007**, *13*, 898–903.
[35] S. Choi, J. Kim, E.-J. Kang, S.-W. Lee, M.-C. Park, Y.-B. Park, S.-K. Lee, *Rheumatology* **2008**, *47*, 1775–1779.
[36] S. Gutierrez, A. Javed, D. K. Tennant, M. van Rees, M. Montecino, G. S. Stein, J. L. Stein, J. B. Lian, *J. Biol. Chem.* **2002**, *277*, 1316–1323.
[37] B. Li, *Endocrine Metab. Immune Disord. Drug Targets* **2008**, *8*, 208–219.
[38] G. Chamberlain, J. Fox, B. Ashton, J. Middleton, *Stem Cells* **2007**, *25*, 2739–2749.
[39] A. Ode, J. Schoon, A. Kurtz, M. Gaetjen, J. E. Ode, S. Geissler, G. N. Duda, *Eur. Cells. Mater.* **2013**, *25*, 37–47.
[40] D. Umulis, M. B. O'Connor, S. S. Blair, *Development* **2009**, *136*, 3715–3728.
[41] H.-M. Ryoo, M.-H. Lee, Y.-J. Kim, *Gene* **2006**, *366*, 51–57.
[42] D. Liu, C. Yi, D. Zhang, J. Zhang, M. Yang, *ACS Nano* **2010**, *4*, 2185–2195.
[43] Y. Yu, M. Zhou, H. Cui, *J. Mater. Chem.* **2011**, *21*, 12622–12625.
[44] R. B. Elmes, K. N. Orange, S. M. Cloonan, D. C. Williams, T. Gunnlaugsson, *J. Am. Chem. Soc.* **2011**, *133*, 15862–15865.